

PCCP

Accepted Manuscript



This article can be cited before page numbers have been issued, to do this please use: M. R. B, N. R. M. V., N. R. Chereddy, B. Shanigaram, B. Kotamarthi, S. Biswas, G. D. Sharma and J. R. Vaidya, *Phys. Chem. Chem. Phys.*, 2016, DOI: 10.1039/C6CP06304G.



This is an Accepted Manuscript, which has been through the Royal Society of Chemistry peer review process and has been accepted for publication.

Accepted Manuscripts are published online shortly after acceptance, before technical editing, formatting and proof reading. Using this free service, authors can make their results available to the community, in citable form, before we publish the edited article. We will replace this Accepted Manuscript with the edited and formatted Advance Article as soon as it is available.

You can find more information about Accepted Manuscripts in the [author guidelines](#).

Please note that technical editing may introduce minor changes to the text and/or graphics, which may alter content. The journal's standard [Terms & Conditions](#) and the ethical guidelines, outlined in our [author and reviewer resource centre](#), still apply. In no event shall the Royal Society of Chemistry be held responsible for any errors or omissions in this Accepted Manuscript or any consequences arising from the use of any information it contains.

Journal Name

ARTICLE

Dithieno[3,2-*b*:2',3'-*d*]pyrrole based, NIR absorbing, solution processable, small molecule donor for efficient bulk heterojunction solar cells.

 Received 00th January 20xx,
Accepted 00th January 20xx

DOI: 10.1039/x0xx00000x

www.rsc.org/

 Manohar Reddy Busireddy,^a Venkata Niladri Raju Mantena,^a Narendra Reddy Chereddy,^{a,*} Balaiah Shanigaram,^b Bhanuprakash Kotamarthi,^{b,*} Subhayan Biswas,^c Ganesh Datt Sharma^{c,*} and Jayathirtha Rao Vaidya^{a,d,*}

A novel, NIR absorbing organic small molecular donor material denoted as **ICT3** with A-D-D-D-A architecture having dithieno[3,2-*b*:2',3'-*d*]pyrrole (DTP) and butylrhodanine as donor and acceptor moieties, respectively is synthesized and its thermal, photophysical, electrochemical and photovoltaic properties are explored. **ICT3** has excellent stability over a broad range of temperatures with the decomposition temperature (T_d corresponds to 5% weight loss) as 372 °C, soluble in most common organic solvents (solubility up to 30 mg/mL) and suitable for solution processing during device fabrication. **ICT3** has broad (520-820 nm) and intense visible region absorption (molar excitation coefficient is $1.69 \times 10^5 \text{ mol}^{-1} \text{ cm}^{-1}$) and has suitable HOMO and LUMO energy levels with [6,6]-phenyl-*C*₇₁-butyric acid methyl ester (PC₇₁BM) acceptor for efficient exciton dissociation and charge transfer. Bulk heterojunction solar cells (BHJSCs) with indium tin oxide (ITO)/poly(3,4-ethylenedioxythiophene):polystyrene sulfonate (PEDOT:PSS)/**ICT3**:PC₇₁BM/poly[(9,9-bis(3'-(*N,N*-dimethylamino)propyl)fluorene-2,7-diyl)-*alt*-(9,9-dioctylfluorene-2,7-diyl)] (PFN)/aluminium (Al) structure are fabricated and the BHJSCs with the active layer as cast from chloroform solution displayed power conversion efficiency (PCE) of 3.04 % ($J_{sc} = 8.22 \text{ mA/cm}^2$, $V_{oc} = 0.86 \text{ V}$ and $FF = 0.43$). Annealing the active layer significantly improved the PCE of these BHJSCs. While thermal annealing the active layer improved the PCE of the BHJSCs to 4.94 %, thermal followed by solvent vapour annealing enhanced the PCE to 6.53 %. X-ray diffraction and atomic force microscopy analyses are carried out on the active layer and these results revealed that annealing treatment improves the crystallinity and nanoscale morphology of the active layer and enrich the device exciton generation and dissociation efficiency, charge transport and collection efficiency and reduces carrier recombination. Observed higher PCE (6.53 %) of the BHJSCs having **ICT3** with DTP donor moiety broaden the scope to develop new, efficient DTP based small molecular donor materials for BHJSCs.

Introduction

In recent years, organic bulk heterojunction solar cells (OBHJSCs) have attracted great interest as an effective technology for using sunlight to produce electricity. Owing to their advantages of low cost, light weight, solution

processability and flexibility, OBHJSCs are considered to be alternative to the conventional silicon solar cells.¹⁻³ In general, bulk heterojunction photoactive layer of OBHJSCs consists of π -conjugated donors (polymer or small molecule) and fullerene acceptors. Broad and efficient light absorption, compatible electronic levels with the fullerene derivatives, efficient charge transport and better thin-film morphology and molecular packing are essential for the donor materials to obtain high power conversion efficiency (PCE).⁴⁻⁸ During the last two decades, numerous efforts have been made to develop new polymer donor materials to enhance the PCE of OBHJSCs and PCE over 10 % has been achieved.⁹⁻¹³ However, drawbacks like difficulties in reproducibility in synthesis, purification and optimization of electronic properties are still associated with polymeric donor materials. Overcoming these limitations, small molecular donor materials have attained

^aCrop Protection Chemicals Division, CSIR-Indian Institute of Chemical Technology, Hyderabad-500007, India. Email: chereddynarendra@gmail.com; jrao@iict.res.in

^bInorganic and Physical Chemistry Division, CSIR-Indian Institute of Chemical Technology, Hyderabad-500007, India

^cDepartment of Physics, The LNM Institute of Information Technology, Jamdoli, Jaipur, India. Email: gdsharma273@gmail.com

^dAcSIR, CSIR-Indian Institute of Chemical Technology, Hyderabad-500007, India

† Footnotes relating to the title and/or authors should appear here.

Electronic Supplementary Information (ESI) available: [NMR, MALDI-MS, absorption and emission spectra and theoretical calculations] See

DOI: 10.1039/x0xx00000x

importance over polymer donor materials in terms of their well-defined molecular weights, excellent reproducibility without batch-to-batch variations, high purity and relatively simple purification procedures.^{4,5} Push-pull organic small molecular donor materials with interconnected electron donating (donor, D) and electron accepting (acceptor, A) moieties can provide broad molecular optical absorption due to intramolecular charge transfer between D and A, assist the formation of favourable morphologies and suitable molecular orbital energy levels.¹⁴⁻²¹ By judicious molecular design of donor materials, morphology control and device optimization, PCE over 10 % has been reported for OBHJSCs with small molecular donor materials.⁶⁻⁸

Short-circuit current density (J_{sc}), open-circuit voltage (V_{oc}) and fill factor (FF) are the main device parameters that influence the PCE of OBHJSCs and high PCE values can be achieved by simultaneously improving the magnitudes of J_{sc} , V_{oc} and FF. Generally, J_{sc} of an OBHJSC can be increased by exploiting donor material with longer wavelength absorption and V_{oc} can be improved by lowering the highest occupied molecular orbital (HOMO) of the donor material to reduce the donor-acceptor recombination.^{22,23} Hence a donor material with low lying HOMO and longer wavelength absorption is advantageous to improve the PCE of an OBHJSC. Optical band gap of push-pull donor materials can be narrowed by selecting the donor moieties with strong electron donating capability to couple with the acceptor moieties. The strong electron donating tendency of the donor moieties can induce efficient electron coupling with acceptors and provide satisfactory long wavelength absorption and high extinction coefficients.²⁴

Recently, benzo[1,2-*b*:4,5-*b'*]dithiophene (BDT) has been widely explored to develop donor materials for high performance OBHJSCs. It is well established that owing to its excellent planarity, fused benzene ring with two peripheral thiophene rings of BDT induces strong intra and intermolecular interactions in its thin film state and improves charge carrier mobility in the bulk heterojunction.^{7,8,25-28} We have also reported two A-D₁-D₂-D₁-A structured BDT (D₂)-dithieno[3,2-*b*:2',3'-*d*]pyrrole (DTP) (D₁)-rhodanine (A) conjugates as donor materials for OBHJSCs.²⁹ By optimizing the device fabrication, we have achieved PCE of 5.90 % for the OBHJSCs using the synthesized donor and [6,6]-phenyl-C₇₁-butyric acid methyl ester (PC₇₁BM) acceptor materials.²⁹ Apart from the advantages of BDT, its poor electron donating tendency limits the absorption profiles of the donor materials to the visible region (< 750 nm).

DTP, a three-ring fused donor moiety has considerable planarity and efficient electron donating capability compared to BDT.³⁰ Considerable efforts have been made by the researchers to describe the utility of DTP based small molecules as donor materials for BHJSCs.^{24,29, 31-45} Roncali and coworkers have reported two D-A-D systems using DTP donor with isoindigo and 3-alkoxy-4-cyanothiophene acceptor units, respectively. BHJSCs fabricated using these donor materials yield moderate efficiencies respectively 0.19 % and 0.88 %.^{33,34} Peter Bauerle and coworkers have reported several A-D-A oligomers comprising DTP as central donor and

dicyanovinylene and thieno[2,3-*c*]pyrrole-4,6-dione units as acceptor moieties. By optimizing various parameters like alkyl side chains and annealing procedures, they have reported PCEs up to 7.1 %.^{36,38,41-43} Recently, Beaujuge and coworkers have reported three DTP-5,6-difluorobenzo-*c*[[1,2,5]thiadiazole (DTP-[2F]BT) small molecule donors with alkyl substituted thiophene end groups having distinct solubilizing side chain and chain length patterns. By optimizing annealing procedures they have achieved PCEs up to 6 %.⁴⁴ Based on these interesting findings on DTP based small molecule donor materials and advantages of DTP moiety,³⁰ we anticipated that synthesis of new donor materials by replacing BDT central donor of our reported donor materials²⁹ with DTP donor can result in a better donor material with improved light harvesting ability.

Considering all the above reasons, herewith we report a new small molecular donor material **ICT3** with A-D-D-D-A architecture containing butylrhodanine acceptor (A) and DTP (D) donor moieties, respectively and its thermal, photophysical, electrochemical and photovoltaic properties are investigated. **ICT3** has good solubility in common organic solvents and has excellent thermal stability. Since DTP has strong electron donating capacity over BDT, **ICT3** has red shifted absorption profile compared to our previously reported BDT based donor materials.²⁹ The broad and intense visible and NIR region absorption and suitable HOMO and LUMO levels of **ICT3** with commonly used acceptor PC₇₁BM allows us to explore its photovoltaic properties. BHJSCs are fabricated using **ICT3** as donor and PC₇₁BM as acceptor materials. BHJSCs fabricated using **ICT3**:PC₇₁BM blends processed from chloroform exhibited PCE of 3.04 % (J_{sc} = 8.22 mA/cm², V_{oc} = 0.86V and FF = 0.43). Annealing the active layer significantly enhanced the PCE of these BHJSCs. The devices with the active layers processed with thermal annealing (TA) and thermal followed by solvent vapour annealing (TA+SVA) showed PCE of 4.94 % and 6.53 %, respectively. The enhancement in PCE of the BHJSCs is attributed to enhanced light harvesting ability and improved nanoscale morphology of the active layer leading to efficient exciton generation, transport and dissociation at the donor-acceptor interface and balanced charge transport to their respective electrodes. Higher PCE (6.53 %) associated with the BHJSCs having **ICT3** with DTP central donor compared to its BDT analogue donor materials²⁹ broadens the scope to develop new, efficient DTP based small molecular donor materials for BHJSCs. Moreover, observed PCE is one among the best reported for DTP based small molecule donors.

Experimental section

Materials and instruments

All the synthetic precursors were obtained from commercial suppliers and used without further purification. Butylrhodanine is synthesized as per the reported procedure.²⁹ Dry toluene (dried on sodium wire), dry DMF (dried over molecular sieves) and freshly distilled THF (distilled over

sodium/benzophenone) were used in all experiments. NMR spectra were recorded using Bruker Avance (500 MHz) spectrometer. MALDI-MS spectra were obtained on a ThermoFinnigan Mass Spectrometer. Absorption spectra were recorded on a Cary 5000 UV-VIS-NIR spectrophotometer. Fluorescence experiments were carried out on a Cary Eclipse fluorescence spectrophotometer. Cyclic voltammetry measurements were conducted on a PC-controlled CHI 62C electrochemical analyzer in CH_2Cl_2 solvent at a scan rate of 100 mV s^{-1} using tetrabutylammonium perchlorate (0.1 M) as supporting electrolyte. The glassy carbon, standard calomel electrode (SCE) and platinum wire were used as working, reference and counter electrodes, respectively. All measurements were carried out at room temperature. The potential of reference electrode was calibrated using ferrocene internal standard. All the potentials were reported against ferrocene. TGA and DSC experiments were conducted under inert atmosphere on Exstar TG/TGA 7200 and Exstar DSC 7020 instruments, respectively with $10 \text{ }^\circ\text{C}/\text{min}$ heating and cooling rate.

Device fabrication and characterization

Small molecule solution processed BHJSCs were fabricated using indium tin oxide (ITO) coated glass as anode electrode and aluminium (Al) as a cathode in the conventional structure of ITO/poly(3,4-ethylenedioxythiophene):polystyrene sulfonate (PEDOT:PSS)/ICT3:PC₇₁BM/poly[(9,9-bis(3'-(*N,N*-dimethylamino)propyl)-2,7-fluorene)-*alt*-2,7-(9,9-dioctylfluorene) (PFN)/Al. The ITO coated glass substrates were pre-cleaned sequentially with aqueous detergent, deionised water, acetone and iso-propanol in ultrasonic bath and finally dried in air. A 40 nm thick PEDOT:PSS layer was spin coated from an aqueous solution onto the ITO coated glass substrate at 3500 rpm and then baked at $110 \text{ }^\circ\text{C}$ for 20 minutes. A blend of ICT3 and PC₇₁BM with different weight ratios was dissolved in a chloroform solution (18 mg/mL) and then spin coated onto a PEDOT:PSS layer to form an active layer. For the thermal annealing of active layer, before the deposition of Al electrode, the layer was annealed at $80 \text{ }^\circ\text{C}$ for 10 minutes. After cooling down to room temperature, the substrates were placed in glass Petri dish containing $100 \mu\text{L}$ THF for 1 minute for solvent vapour annealing (SVA). PFN cathode buffer layer was prepared directly by spin coating the PFN in methanol solution on the top of active layer, without any additional thermal annealing or post treatment. Finally, 90 nm of Al was deposited by thermal evaporation at high vacuum of 10^{-5} Torr on the top of active layer to complete the device. For the hole-only devices, the diode was fabricated with a ITO/PEDOT:PSS/active layer/Au configuration using a process similar to that used for the photovoltaic cells described above. Only the top electrode (Au, 90 nm) was vacuum-deposited on the active layer (10^{-5} Torr). The electron-only devices were fabricated with an Al/active layer/Al structure. The current-voltage characteristics of the photovoltaics were measured using a computer-controlled Keithley 2400 source meter under illumination intensity of 100

mW/cm^2 . A solar simulator consist of a xenon light source coupled with an AM 1.5 optical filter was used as the light source to illuminate the surface of the devices. The incident photons to current conversion efficiency (IPCE) measurements were performed at zero bias by illuminating the device with monochromatic light supplied from a Xenon arc lamp in combination with a monochromator. The number of photons incident on the sample was calculated for each wavelength by using a silicon photodiode. The resulting current was measured by the Keithley electrometer under short circuit conditions. The J-V characteristics of the hole only and electron only devices were measured in the range of 0-3 V using a Keithley 2400 source measuring unit in the dark. The carrier mobility was calculated by fitting the J-V curves to a space charge limited current (SCLC) model.

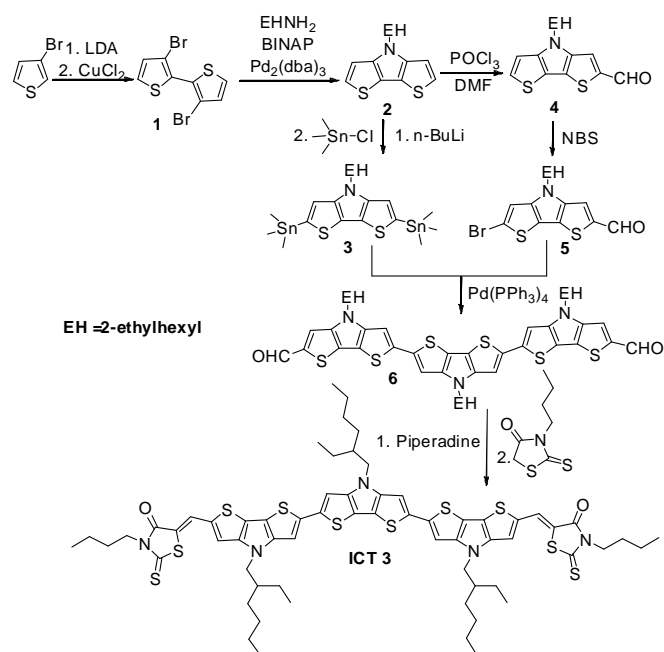
Synthetic procedures

3,3'-Dibromo-2,2'-dithiophene (1):

Intermediate **1** is synthesized by modifying the reported procedure.⁴⁶ The freshly prepared LDA solution [prepared by the addition of *n*-BuLi (2.5 M in hexanes, 100 mmol, 40 mL) and diisopropylamine (0.110 mol, 11.1 g) in 50 mL of anhydrous THF ($-78 \text{ }^\circ\text{C}$ to room temperature)] was added drop wise to a solution of 3-bromothiophene (16.30 g, 100 mmol) in anhydrous THF (100 mL) at $-78 \text{ }^\circ\text{C}$ under nitrogen atmosphere. After the solution was stirred for 5 minutes, white precipitate was formed. The reaction mixture was stirred for 1 h at $-78 \text{ }^\circ\text{C}$ followed by the addition of CuCl_2 (14.11 g, 105 mmol) in one portion. The dark coloured reaction mixture was allowed to warm up to room temperature and treated with aqueous HCl. The organic phase separated was collected and the aqueous phase was extracted with diethyl ether for several times. The combined organic phase was dried over anhydrous Na_2SO_4 and the solution was filtered, concentrated and the residue obtained was purified by silica gel column chromatography (eluent: hexane) to afford a white solid (yield 85%). NMR data obtained is matched well with the literature reports.⁴⁷ ^1H NMR (500 MHz, CDCl_3 , δ ppm): 7.08 (d, $J = 5.0$ Hz, 2H), 7.40 (d, $J = 5.0$ Hz, 2H); ^{13}C NMR (125 MHz, CDCl_3 , δ ppm): 112.6, 127.5, 128.8, 130.7. EI-MS (Positive mode, m/z): 324 (M^+), Calc. for $\text{C}_8\text{H}_4\text{Br}_2\text{S}_2$ is 324. Melting point: $97\text{-}99 \text{ }^\circ\text{C}$

N-(2-Ethylhexyl)-dithieno[3,2-*b*:2',3'-*d*]pyrrole (2):

Intermediate **2** is synthesized by modifying the reported procedure.⁴⁶ A solution of compound **1** (10.0 g, 30.86 mmol), sodium *tert*-butoxide (7.41 g, 77.14 mmol), $\text{Pd}_2(\text{dba})_3$ (1.41 g, 1.54 mmol) and 2,2'-bis (diphenylphosphino)-1,1'-binaphthyl (BINAP, 1.92 g, 3.1 mmol) in anhydrous toluene (120 mL) was purged with N_2 gas for 10 minutes and 2-ethylhexylamine (3.98 g, 30.85 mmol) was added *via* syringe. The mixture was refluxed overnight with continuous stirring under N_2 atmosphere. The reaction was quenched by adding cold water (150 mL) and the layers formed were separated. The aqueous phase was extracted with CH_2Cl_2 for three times. The combined organic layers was washed with water twice and



Scheme 1. Scheme for the synthesis of ICT3.

then dried over anhydrous Na_2SO_4 . After the removal of solvent under reduced pressure, the residue was purified by column chromatography on silica gel (eluent: CH_2Cl_2 /petroleum ether, 1/6 v/v) to provide the title compound as a yellow oil (yield 90%). NMR data obtained is matched well with the literature reports.⁴⁸

^1H NMR (500 MHz, CDCl_3 , δ ppm): 0.81-0.94 (m, 6H), 1.20-1.40 (m, 8H), 1.89-2.00 (m, 1H), 4.00-4.11 (m, 2H), 6.98 (d, $J = 6.5$ Hz, 2H), 7.12 (d, $J = 6.5$ Hz, 2H); ^{13}C NMR (125 MHz, CDCl_3 , δ ppm): 10.7, 14.0, 22.9, 24.0, 28.6, 30.6, 40.4, 51.3, 111.0, 114.5, 122.6, 145.3. ESI-MS (Positive mode, m/z): 292.20 ($\text{M}+\text{H}^+$), Calc. for $\text{C}_{16}\text{H}_{22}\text{NS}_2$ is 292.12.

N-(2-Ethylhexyl)-2,6-bis(trimethylstannyl)dithieno[3,2-*b*:2',3'-*d*]pyrrole (3):

To the solution of compound **2** (1.02 g, 3.5 mmol) in dry THF (250 mL) at -78 °C, *n*-BuLi (2.5 M in hexane, 3.0 mL, 7.5 mmol) was added under N_2 atmosphere. The resulting solution was stirred for 1 h at -78 °C and then slowly warmed to room temperature and stirred for an additional hour. The reaction mixture was again cooled to -78 °C and trimethyltin chloride (1 M in hexane, 8.0 mL, 8.0 mmol) was added in one portion. After addition, the mixture was warmed to room temperature and stirred for 3 h. The reaction was quenched by adding water and extracted with diethyl ether. The combined organic extract was washed with brine and then dried over anhydrous Na_2SO_4 . The resulting solution was filtered and the solvent was removed under vacuum to obtain the title compound as dark brown liquid (yield 90%). The product obtained was used as it is for next step.

^1H NMR (500 MHz, CDCl_3 , δ ppm): 0.39 (s, 18H), 0.85-0.95 (m, 6H), 1.24-1.42 (m, 8H), 1.94-2.02 (m, 1H), 4.00-4.11 (m, 2H), 6.96 (s, 2H); ^{13}C NMR (125 MHz, CDCl_3 , δ ppm): -8.1, 10.7, 14.1, 23.0, 24.0, 28.4, 30.5, 40.3, 51.3, 118.0, 120.1, 135.5, 148.2. ESI-MS (Positive mode, m/z): 617 (M^+), Calc. for $\text{C}_{22}\text{H}_{37}\text{NS}_2\text{Sn}_2$ is 617.

N-(2-Ethylhexyl)-4*H*-dithieno[3,2-*b*:2',3'-*d*]pyrrole-2-carbaldehyde (4):

To the solution of **2** (5.0 g, 17.2 mmol) in ethylene dichloride (150 mL) in a 250 mL round bottom flask, dry DMF (1.38 g, 18.90 mmol) was added at room temperature. The resulting solution was cooled to 0 °C and POCl_3 (4.8 mL, 51.5 mmol) was added drop wise. The reaction mixture was allowed to warm to room temperature and refluxed overnight. On the following day, the reaction mixture was cooled down to room temperature and worked up with saturated sodium acetate and chloroform. The organic layer collected was washed with water and brine and dried over anhydrous Na_2SO_4 . The solution was filtered and concentrated to get crude yellow oil, which was purified by column chromatography on silica gel (10 % ethyl acetate/hexane) to give the title compound (yield 76%) as a dark yellow oil.

^1H NMR (500 MHz, CDCl_3 , δ ppm): 0.82-0.97 (m, 6H), 1.20-1.40 (m, 8H), 1.92-2.00 (m, 1H), 4.05-4.15 (m, 2H), 7.00 (d, $J = 5.5$ Hz, 1H), 7.38 (d, $J = 5.5$ Hz, 1H), 7.63 (s, 1H), 9.88 (s, 1H); ^{13}C NMR (125 MHz, CDCl_3 , δ ppm): 10.6, 13.9, 22.9, 24.0, 28.6, 30.6, 40.4, 51.4, 111.0, 114.8, 119.4, 123.1, 128.4, 139.9, 144.6, 149.5, 182.9. ESI-MS (Positive mode, m/z): 320.15 ($\text{M}+\text{H}^+$), Calc. for $\text{C}_{17}\text{H}_{22}\text{NOS}_2$ is 320.11.

6-Bromo-4-(2-ethylhexyl)-4*H*-dithieno[3,2-*b*:2',3'-*d*]pyrrole-2-carbaldehyde (5):

To a stirred solution of **4** (3.2 g, 10 mmol) in THF (100 mL) protected from sun light at 0 °C, NBS (1.96 g, 11 mmol) was added portion wise. After complete addition, reaction mixture was warmed to room temperature and stirred overnight in the dark. After the completion of reaction, water (50 mL) was added and the solution was extracted with chloroform. The organic phase was washed with water and dried over anhydrous Na_2SO_4 . The resulting solution was filtered and solvent was removed under reduced pressure. The crude product was purified on a silica gel column with 10 % ethyl acetate/hexane as eluent to obtain the title compound as a yellow solid (yield 95%).

^1H NMR (500 MHz, CDCl_3 , δ ppm): 0.83-0.96 (m, 6H), 1.21-1.40 (m, 8H), 1.84-1.98 (m, 1H), 3.99-4.11 (m, 2H), 7.05 (s, 1H), 7.60 (s, 1H), 9.87 (s, 1H); ^{13}C NMR (125 MHz, CDCl_3 , δ ppm): 10.6, 13.9, 22.9, 23.9, 28.5, 30.5, 40.3, 51.4, 114.3, 114.8, 115.4, 119.4, 122.7, 140.2, 143.5, 146.8, 182.9. ESI-MS (Positive mode, m/z): 400.10 ($\text{M}+\text{H}^+$), Calc. for $\text{C}_{17}\text{H}_{21}\text{BrNOS}_2$ is 398.02. Melting point: 93-95 °C

2,2':6',2''-Ter(*N*-(2-ethylhexyl)dithieno[3,2-*b*:2',3'-*d*]pyrrole)-6,6''-dicarbaldehyde (6):

A solution of compound **3** (1.29 g, 3.23mmol) and **5** (1 g, 1.295mmol) in dry toluene (20 mL) was degassed twice with N₂ gas followed by the addition of Pd(PPh₃)₄ (374 mg, 0.323 mmol). After being stirred at 100 °C for 24 h under N₂ atmosphere, the reaction mixture filtered through celite powder and extracted with CH₂Cl₂. The organic layer was washed with water and then dried over anhydrous Na₂SO₄. After removal of solvent, the crude product was purified by column chromatography on silica gel using a mixture of dichloromethane and petroleum ether (2:1) as eluent to afford compound as a red solid (yield 70%).

¹H NMR (500 MHz, CDCl₃, δ ppm): 0.85-1.01 (m, 18H), 1.25-1.44 (m, 24H), 1.90-2.01 (m, 3H), 3.99-4.14 (m, 6H), 6.98 (s, 2H), 7.06 (s, 2H), 7.52 (s, 2H), 9.83 (s, 2H); ¹³C NMR (125 MHz, CDCl₃, δ ppm): 10.7, 10.8, 14.0, 14.1, 23.0, 23.1, 24.1, 28.6, 30.6, 40.4, 51.2, 51.3, 105.7, 107.4, 113.0, 114.4, 119.1, 123.1, 135.8, 139.9, 141.3, 144.3, 145.3, 149.4, 182.6. MALDI-MS (Positive mode, m/z): 925.24 (M⁺), Calc. for C₅₀H₅₉N₃O₂S₆ is 925.29. Melting point: 194-196 °C

(5Z,5'Z)-5,5'-[[2,2':6',2''-Ter(*N*-(2-ethylhexyl)dithieno[3,2-*b*:2',3'-*d*]pyrrole)-6,6''-diyl]bismethylene]bis(3-butyl-2-thioxo-4-thiazolidinone) (ICT3):

To the solution of **6** (1.08 g, 1 mmol) in chloroform (30 mL), butylrhodanine (0.76 g, 4 mmol) and catalytic amount of piperidine were added under inert atmosphere and the resulting solution was refluxed overnight. The reaction mixture was cooled down to room temperature and partitioned between water and chloroform and the chloroform layer was collected. The aqueous layer was washed with chloroform (3 x 25 mL) and the combined organic extract was washed with brine. The organic extract was dried over anhydrous Na₂SO₄, filtered and concentrated under reduced pressure. The crude obtained was purified on silica gel column chromatography (30 % chloroform in hexane as eluent) to yield the title compound as green-black solid (yield 80%)

¹H NMR (500 MHz, CDCl₃, δ ppm): 0.89-1.02 (m, 24H), 1.28-1.46 (m, 28H), 1.63-1.74 (m, 4H), 1.90-2.00 (m, 3H), 3.95-4.12 (m, 10H), 6.91 (s, 2H), 6.95 (s, 2H), 7.11 (s, 2H), 7.80 (s, 2H); ¹³C NMR (125 MHz, CDCl₃, δ ppm): 10.78, 10.82, 13.67, 14.13, 20.10, 23.07, 24.12, 28.61, 28.68, 29.02, 29.68, 30.57, 30.63, 40.42, 44.54, 51.32, 105.21, 106.83, 113.32, 114.15, 116.17, 116.83, 122.79, 126.66, 135.07, 135.88, 140.84, 145.39, 145.53, 148.36, 167.25, 191.87. MALDI-MS (Positive mode, m/z): 1267.78 (M⁺), Calc. for C₆₄H₇₇N₅O₂S₁₀ is 1267.32.

Results and discussion

Synthesis and thermal properties

Chemical structure of **ICT3** is shown in **scheme 1**. The donor material **ICT3** has A-D-D-D-A architecture and contains DTP and butylrhodanine as donor and acceptor moieties, respectively. Synthetic scheme of **ICT3** is shown in **scheme 1** and its detailed synthetic procedures are provided in the experimental section. The reported **ICT3** was synthesized by condensing the bis-aldehyde intermediate **6** with butylrhodanine. The bis-aldehyde intermediate **6** was obtained

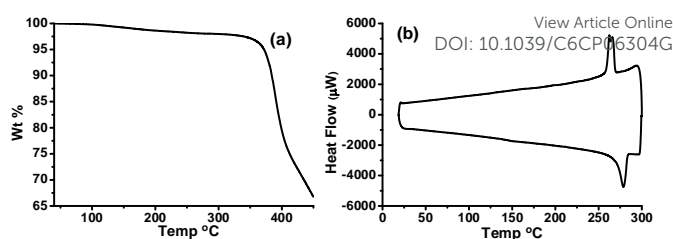


Fig. 1. TGA (a) and DSC (b) thermograms of **ICT3**

from the corresponding distannyl derivative **3** and **5**. Intermediate **3** was synthesized by lithiation of **2** using *n*-BuLi followed by quenching with trimethyltin chloride. Intermediate **2** was prepared by Pd⁰-catalyzed Buchwald-Hartwig coupling of **1** and 2-ethylhexylamine. Intermediate **5** was synthesized from **2**, by subjecting it for formylation using POCl₃/DMF followed by bromination with NBS. All the intermediates and the donor molecule **ICT3** are thoroughly characterised (Figs. S1-S3, and Figs. S8-S26, ESI†). **ICT3** is soluble in common organic solvents and suitable for solution processability during device fabrication.

Thermal properties and phase transition characteristics of **ICT3** were evaluated using thermo-gravimetric analysis (TGA) and differential scanning calorimetry (DSC), respectively, under nitrogen atmosphere at a heating rate of 10 °C/min. TGA and DSC thermograms of **ICT3** are shown in **Fig. 1** and the corresponding data is provided in **Table 1**. From the TGA analysis, it is clear that **ICT3** has good thermal stability with the decomposition temperature (T_d , defined as that at which 5 % wt loss is observed) of 372 °C (**Fig. 1a**). During the DSC analysis, **ICT3** exhibits a sharp endotherm corresponding to its melting temperature (T_m) at 278 °C (**Fig. 1b**). High T_d and T_m observed for **ICT3** designates its applicability even at elevated temperatures. Moreover, in the DSC analysis, multiple crystallization exotherms are observed during the first cooling cycle supporting the highly crystalline nature of **ICT3** and it could be due to the strong intermolecular interactions among the **ICT3** molecules induced by the flat DTP donor moiety.⁴⁹

Photophysical and electrochemical properties

The UV-Visible absorption characteristics of **ICT3** were measured both in solution and thin film states. **Fig. 2a** shows the UV-Visible absorption spectra of **ICT3** and the corresponding data is provided in **Table 2**. In chloroform solution, **ICT3** displays absorption bands in two distinct regions, i.e. 300-500 nm and 500-750 nm. Absorption band at longer wavelength has absorption maximum (λ_{max}) at 630 nm with an extinction coefficient (ϵ) of $1.69 \times 10^5 \text{ M}^{-1} \text{ cm}^{-1}$ (**Fig. 2a**

Table 1. Thermal data of **ICT3**.

Material Code	Decomposition temperature (T_d) °C	Melting temperature (T_m) °C	Crystallization temperature (T_c) °C
ICT3	372	278	262, 266

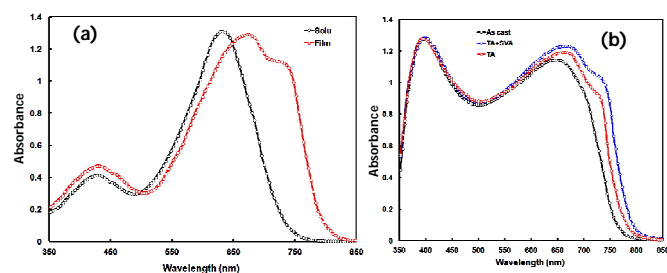


Fig. 2. UV-visible absorption spectra of **ICT3** in chloroform solution (10 μM) and in thin films (a) and Absorption spectra of as cast and annealed **ICT3:PC₇₁BM** blend thin films (b).

and **Table 2**). Observed high ϵ is attributed to the planarity of the molecular backbone of **ICT3**. Compared to ter(DTP) donor core alone reported by Roncali and coworkers, absorption band of **ICT3** is red shifted by ~ 166 nm (**Table 2**), indicating intramolecular charge transfer among the DTP donor and rhodanine acceptor units.⁵⁰ Moreover, the broad and red shifted absorption of **ICT3** compared to its **BDT** analogue materials (Fig. S4, ESI[†]) supports the efficient electron donating tendency of DTP compared to **BDT** unit. It can be seen that, absorption bands of **ICT3** in thin film state are red shifted about 40 nm with a new vibronic shoulder peak at longer wavelength regions (**Fig. 2a**), indicating the strong intermolecular interactions due to π -stacking and effective intermolecular packing between the molecular backbones.⁵¹⁻⁵³ These intermolecular interactions are beneficial for efficient charge transport. The optical band gap of **ICT3** calculated from the absorption onset of thin film is estimated to be 1.56 eV and it falls in the optimal range (1.5-1.6 eV) to obtain best PCE.⁵⁴ Moreover, the broad and NIR (510-830 nm) light harvesting capacity of **ICT3** compared to its **BDT** analogues can improve the exciton generation efficiency and short circuit current density (J_{sc}) of the corresponding BHJSCs.

Absorption spectra of **ICT3:PC₇₁BM** blend film processed from chloroform solvent under different conditions are shown in **Fig. 2b**. Absorption spectra of **ICT3:PC₇₁BM** blend film as cast from chloroform solvent comprised two characteristic bands, one at shorter wavelength corresponding to **PC₇₁BM** and another at longer wavelength corresponding to **ICT3**. However, compared to the pristine films (**Fig. 2a**), the absorption band corresponding to **ICT3** in their blend film is considerably blue shifted with disappearance of vibronic peak shoulder indicating the strong interaction between the **ICT3** and **PC₇₁BM**

Material Code	λ_{max} (nm) ^a	ξ ($\times 10^5 \text{ Mol}^{-1} \text{cm}^{-1}$)	λ_{max} (nm) ^b	E_{HOMO} (eV) ^c	E_{LUMO} (eV) ^d	E_{ox} (V)	E_{HOMO} (eV)	E_{LUMO} (eV) ^e
ICT3	630	1.69	670	1.77	1.56	0.13	-5.16	-3.39
Ter(DTP) ^f	464	0.55	468	2.27	-	0.04	-5.14	-

Table 2. Photophysical and electrochemical data of **ICT3**.

^ain dilute chloroform solution (10 μM), ^bin thin film cast from chloroform solution, ^cestimated from intersection of absorption and emission spectra in chloroform solution, ^destimated from $E_{\text{g}}^{\text{opt}} = 1240/\lambda_{\text{onset}}$, λ_{onset} is onset absorption wavelength in thin film, ^e $E_{\text{LUMO}} = E_{\text{HOMO}} - E_{\text{O-O}}$, ^fvalues are reported from reference 50

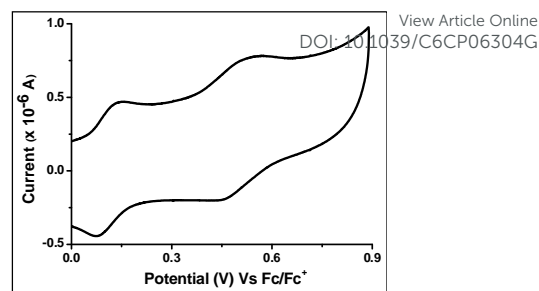


Fig. 3. Cyclic voltammogram represent quasi-reversible oxidation behaviour of **ICT3**

that disrupt the intermolecular packing of **ICT3** molecules. Annealing (TA or TA+SVA) the blend film broadened and red shifted the absorption band corresponding to **ICT3** with a new vibronic shoulder as observed in their pristine films revealing that annealing treatment improves the molecular packing of **ICT3** in their blend films.

Redox properties of **ICT3** were studied using cyclic voltammetry (CV) analysis to estimate its HOMO (highest occupied molecular orbital) and LUMO (lowest unoccupied molecular orbital) energy levels. Cyclic voltammogram of **ICT3** is shown in **Fig. 3** and it shows two quasi-reversible one-electron oxidation waves with onset oxidation potentials 0.06 and 0.40 V vs. Fc/Fc^+ (0.36 and 0.70 V vs SCE) corresponding to cation radical and dicationic states of **ICT3**, respectively. Obtained oxidation peak potential values (0.43 and 0.81 V vs SCE) are comparable with ter(DTP) (0.34 and 0.71 V vs SCE) reported by Roncali and coworkers.⁵⁰ The HOMO energy level of **ICT3** was calculated from the onset oxidation potential by assuming that energy level of Fc/Fc^+ to be -5.1 eV below the vacuum level. The LUMO energy level of **ICT3** was estimated from $E_{\text{LUMO}} = E_{\text{HOMO}} - E_{\text{O-O}}$, where $E_{\text{O-O}}$ was obtained from the intersection of solution state absorption and emission spectra (Fig. S5, ESI[†]). The HOMO and LUMO energy level values of **ICT3** are provided in **Table 2**. Higher magnitude of the HOMO energy of **ICT3** compared to its **BDT** analogues reported also supports the higher electron donating capacity of DTP moiety over **BDT** unit (Fig. S4, ESI[†]). Since open-circuit voltage of a BHJSC depends on the energy difference between the HOMO of the donor and LUMO of the acceptor material, observed increase in the HOMO of the **ICT3** compared to its **BDT** analogues can reduce the V_{oc} of BHJSC devices. However, well aligned HOMO and LUMO energy levels of **ICT3** with the HOMO (-6.0 eV) and LUMO (-4.1 eV) levels of **PC₇₁BM** designates its suitability as a donor material in BHJSCs when blended with **PC₇₁BM** acceptor. Since the energy gap of the donor-acceptor LUMO levels has prominent role on the exciton dissociation, observed 0.71 eV higher magnitude of the LUMO of **ICT3** over **PC₇₁BM** can afford effective photo-induced charge separation at D/A interface.⁵⁵

Theoretical studies

Theoretical calculations were performed to understand the molecular level properties of **ICT3** using density functional

theory (DFT) and time dependant density functional theory (TD-DFT). Ground state geometry of **ICT3** was fully relaxed in gas phase without any symmetry constraints during relaxation. Geometry optimization was performed using B3LYP, a hybrid exchange-correlation functional along with 6-31G(d,p) basis set.⁵⁶⁻⁶¹ Frequency analysis was carried out to confirm that the relaxed geometries are the local minima on the potential energy surface. Relaxation process was done according to the default tight convergence criteria implemented in the G09 package. Long alkyl chains were replaced with methyl groups for computational ease. Vertical excitation energy of **ICT3** was estimated for the first 25 states using TD-DFT method using PBE, B3LYP and M06 functionals and 6-31G(d,p) basis set over the ground state optimized geometry.^{56-58,62,63} Solvent effects were also included for chloroform (CF) solvent using the integral equation formalism variant of the polarisable continuum model (IEFPCM) as implemented in the Gaussian package.^{64,65} Molecular orbital analysis was performed on **ICT3** to estimate the electron density distribution over different fragments in various MOs. Gausssum package was used to estimate the percentage contribution of various fragments to the corresponding FMOs.⁶⁶ All these calculations were performed using G09 software package.

As shown in the Fig. S6, ESI†, optimized structure of **ICT3** is almost planar and the dihedral angle between the central DTP molecular plane and the peripheral DTP molecular plane of **ICT3** is in the range of 8.34-14.67°. This high planarity of **ICT3** assists the formation intermolecular aggregates and it could be the reason for the observed wavelength shift and new vibronic bands in the thin film absorption spectrum of **ICT3** (Fig. 2a). The HOMO and LUMO energy levels and allowed vertical electronic excitations of **ICT3** were calculated using M06, B3LYP and PBE functionals and the results obtained are provided in Tables S1-S3, ESI†. From these results it is clear that HOMO→LUMO transition has predominant contribution to the first excitation. Optimized structures, isosurface plots of

the frontier molecular orbitals (FMOs) of **ICT3** are shown in Fig. 4. It is clear from Fig. 4 that, the HOMO and LUMO of **ICT3** are extended all over the molecular backbone. However, the HOMO is more localized on central and peripheral DTP donor moieties and the LUMO is predominant on peripheral DTP and butylrhodanine moieties. Results obtained from the Gausssum package revealing the contributions of different moieties of **ICT3** to its FMOs is shown in the Fig. S7, ESI†. Since HOMO→LUMO transition is mainly contributed to the first excited state, moderate charge transfer from the central and peripheral DTP donor moieties to the butylrhodanine acceptor moiety is observed. UV-Visible absorption spectra of **ICT3** obtained using TD-DFT analysis (M06/6-31G(d,p) and B3LYP/6-31G(d,p)) in gas and chloroform solvent phases are shown in Fig S8, ESI†. These absorption spectra were acquired by convoluting Gaussian functions with FWHM as 3000 cm⁻¹ using Gausssum package. The absorption spectra generated from the gas phase studies are in good agreement with the experimental results. However, the absorption maxima of **ICT3** obtained from TD-DFT calculations in chloroform solvent phase is slightly overestimated.

Photovoltaic properties

In order to evaluate the photovoltaic properties of **ICT3**, bulk heterojunction solar cells were fabricated using **ICT3** as donor and PC₇₁BM as acceptor materials with a conventional device structure of ITO/PEDOT:PSS/**ICT3**:PC₇₁BM/PFN/AI. Initially, BHJSCs were optimized by fabricating the devices with various D/A weight ratios of 1:1, 1:1.5, 1:2 and 1:2.5 in chloroform solution keeping the total concentration as 18 mg/mL. We found that devices based on **ICT3**:PC₇₁BM (1:2 wt ratio) show best photovoltaic performance and all the further studies were carried out using 1:2 D/A weight ratio. Current-voltage characteristics and incident photon to current conversion efficiency (IPCE) spectra of the devices with optimized **ICT3**:PC₇₁BM active layer are shown in Fig. 5 and the corresponding photovoltaic parameters are summarized in Table 3. The device fabricated from the active layer processed with chloroform solution showed a PCE of 3.04 % with J_{sc} of 8.22 mA/cm², V_{oc} of 0.86 V and FF of 0.43. The IPCE spectra consist of two bands (Fig. 5b) and closely resembles with the absorption spectra of active layer. The band at shorter and longer wavelength regions corresponds to the absorption of PC₇₁BM and **ICT3**, respectively indicating that the both PC₇₁BM and **ICT3** contribute to the photocurrent generation. The overall PCE of the solar cell based on **ICT3**:PC₇₁BM processed with chloroform is quite low and it could be due to the poor J_{sc}

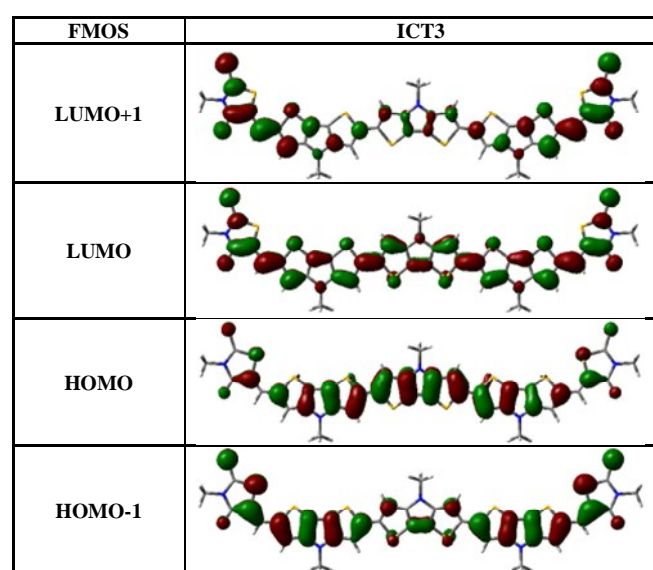


Fig. 4. FMO distributions of **ICT3**.

Active layer	J _{sc} (mA/cm ²)	V _{oc} (V)	FF	PCE (%)	J _{sc} (mA/cm ²) ^b
ICT3 :PC ₇₁ BM (as cast)	8.22	0.86	0.43	3.04 (2.97) ^c	8.14
ICT3 :PC ₇₁ BM (TA)	10.38	0.82	0.58	4.94 (4.88) ^c	10.32
ICT3 :PC ₇₁ BM (TA+SVA)	11.94	0.84	0.65	6.53 (6.47) ^c	11.86

Table 3. Photovoltaic parameters of the BHJSC devices based on **ICT3**.

^bEstimated from IPCE spectra of devices

^cAverage of 8 devices

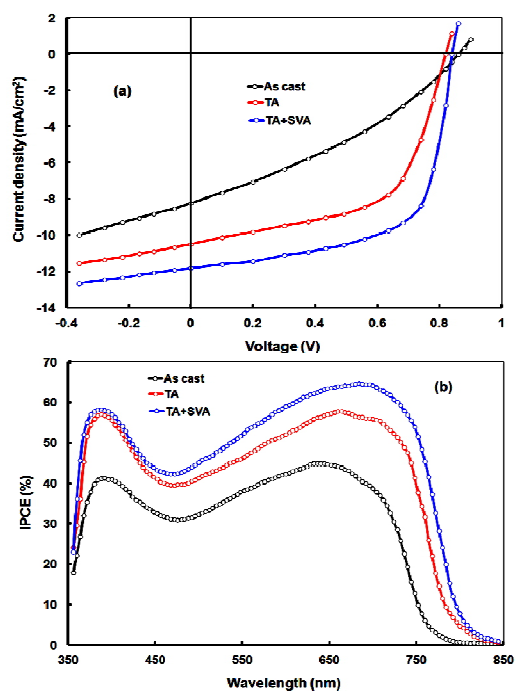


Fig. 5. Current–voltage characteristics under illumination (a) and incident photon to current conversion efficiency (IPCE) spectra (b) of the devices processed under different conditions

and FF associated with these devices. Since thermal annealing (TA)^{7,67,68} and solvent vapour annealing (SVA)^{69–71} can improve the morphology of the active layer and thereby enhances the PCE of the device, we have fabricated BHJSCs based on the thermal annealed (TA) and thermal followed by solvent vapour annealed (TA+SVA) active layers. Current–voltage characteristics and IPCE spectra of these devices are also included in **Fig. 5**. The BHJSCs with the active layer treated with TA exhibited a better PCE of 4.94 % with J_{SC} of 10.38 mA/cm², V_{OC} of 0.82 V and FF of 0.58. With simultaneous TA and SVA treatment of the active layer, PCE is further increased to 6.53 % with J_{SC} of 11.94 mA/cm², V_{OC} of 0.84 V and FF of 0.65 (**Table 3**). BHJSC devices with ICT3 donor displayed higher J_{SC} and FF and lower V_{OC} values compared to the BHJSCs with its BDT analogue donor materials (**Fig. S4**, ESI†). These results are in agreement with the photophysical and electrochemical data obtained for ICT3. Since ICT3 has broad and red shifted optical absorption compared to its BDT analogues, higher exciton generation is expected and that in turn could improve the J_{SC} of the devices. Observed decrease in the V_{OC} values of the BHJSCs with ICT3 donor could be due to its higher magnitude HOMO level compared to its BDT analogues. However overall PCE of the BHJSCs with ICT3 donor is higher compared to the BHJSCs with its BDT analogue donor materials (**Fig. S4**, ESI†). Hence it is clear that replacing BDT with DTP can result in the donor materials with better photovoltaic properties.

In order to get insights about the increase PCE of the BHJSCs with annealed active layer, we have measured the hole and electron mobilities in the active layers by measuring the J–V characteristics of the hole and electron only devices and fitting these characteristics with space charge limited current described by Mott–Gurney model.⁷² The J–V characteristics of

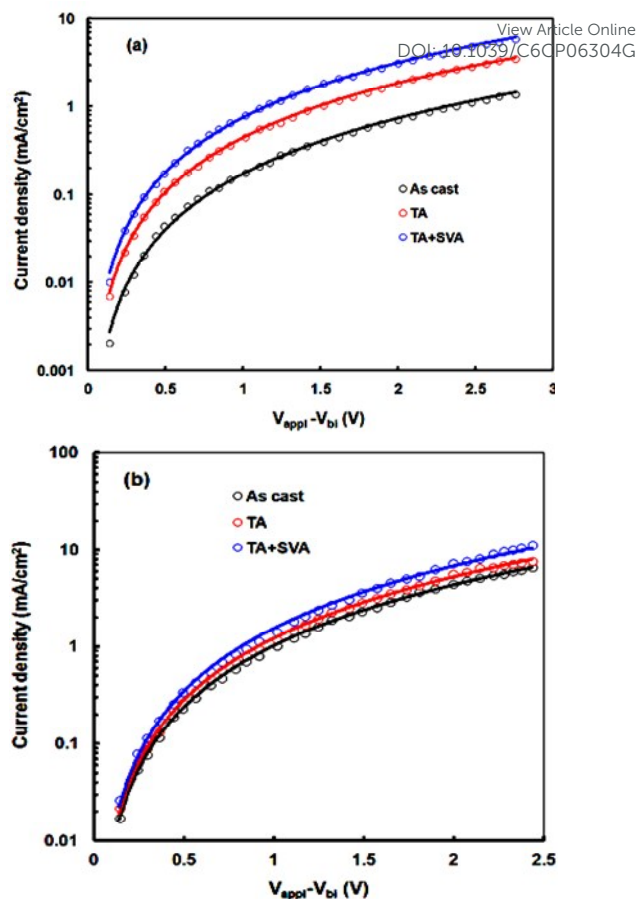


Fig. 6. Current–voltage characteristics in dark for hole (a) and electron (b) only devices, solid lines indicates SCLC fitting.

the hole and electron only devices are shown in **Fig. 6a** and **6b**, respectively. The device with active layer spin cast from chloroform solvent exhibited hole (μ_h) and electron (μ_e) mobilities as 2.64×10^{-5} and 2.48×10^{-4} cm²/Vs, respectively with the electron to hole mobility ratio (μ_e/μ_h) of 9.34 leading to the unbalanced charge transport and could be the reason for the observed low PCE (3.04 %) of the BHJSCs with as cast active layer. Interestingly, annealing treatment on the active layer substantially improved the hole mobility of the devices. Devices with TA treated active layer displayed the μ_h and μ_e as 9.54×10^{-5} and 2.43×10^{-4} cm²/Vs, respectively with the $\mu_e/\mu_h = 2.55$. Devices with TA+SVA treated active layer showed further enhancement in the μ_h and the observed μ_h and μ_e are 1.76×10^{-4} and 2.54×10^{-4} cm²/Vs, respectively and μ_e/μ_h is 1.44. Hence these results clearly indicate that annealing treatment imparts balanced charge transport in the active layer and in turn reduce the charge recombination and leads to an increase in FF, J_{SC} , and overall PCE of the BHJSCs.

We have also measured the photocurrent density (J_{ph}) and effective voltage (V_{eff}) characteristics of the BHJSCs with the ICT3:PC₇₁BM active layer processed under different conditions and the data is shown in **Fig. 7**. As shown in the **Fig. 7**, J_{ph} ($J_{ph} = J_L - J_D$, where J_L and J_D are the current densities under illumination and in dark, respectively) of the BHJSCs is increased sharply with V_{eff} ($V_{eff} = V_o - V_{appl}$, where V_{appl} is the

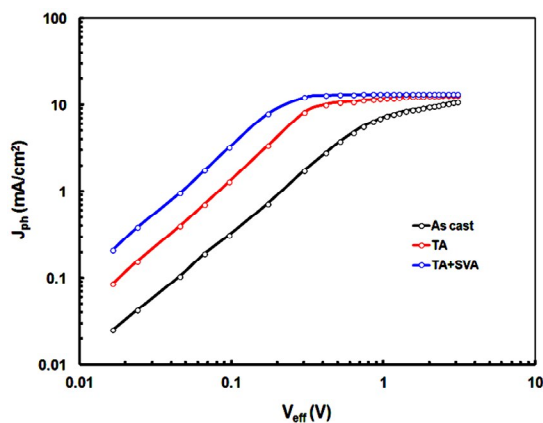


Fig. 7 Photocurrent density (J_{ph}) versus effective voltage (V_{eff}) characteristics for the devices with as cast from CF, TA and TA+SVA treated ICT3:PC₇₁BM active layers under constant incident light intensity (AM 1.5G, 100 mW/cm²).

applied voltage and V_0 is the voltage at which $J_{ph} = 0$ ⁷³ and reached to a saturated value (J_{phsat}) at higher V_{eff} . However, the increment in the J_{ph} with respect to V_{eff} is sharp for the BHJSCs with TA or TA+SVA treated active layer and reached J_{phsat} at low value of V_{eff} compared to the BHJSCs with as cast active layer. These results suggested that for the BHJSCs with either TA and TA+SVA treated active layers, both the exciton generation, their dissociation into free charge carriers and charge collection at the respective electrodes are more efficient compared to the BHJSCs with as cast active layer. Since J_{phsat} is correlated to the maximum exciton generation rate, which is a measure of the maximum number of photon absorbed,^{74,75} higher J_{phsat} observed for the BHJSCs with TA+SVA treated active layer indicates the higher light harvesting capacity of these devices. These results are also consistent with the UV-Visible absorption of the active layers (Fig. 2b). Moreover, we observed a significant enhancement in the J_{ph}/J_{phsat} ratio at short circuit conditions for the BHJSCs with annealing treated active layer (0.84 and 0.89, respectively for TA and TA+SVA treated active layer) over the BHJSCs with as cast active layer (0.72). Since the J_{ph}/J_{phsat} ratio is related to the overall exciton dissociation and charge collection efficiencies, observed higher magnitudes of the J_{ph}/J_{phsat} values for the BHJSCs with annealing treated active layer indicate their improved charge collection efficiency.⁷¹ Hence the results

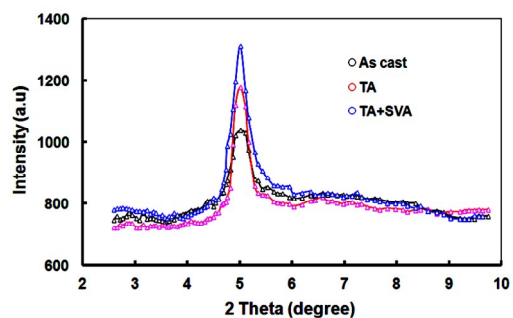


Fig. 8 XRD patterns of the active layer thin films processed under different conditions.

of the hole/electron mobility experiments and $J-V$ characteristics collectively suggested that TA+SVA treatment of active layer improves the exciton generation and dissociation efficiency, charge transport and collection efficiency and reduces the carrier recombination of the BHJSCs.

Since the annealing treatment substantially altered the absorption (Fig. 2b) and charge transport characteristics (Fig. 6 and Fig. 7) of the active layer, we expected that observed significant enhancement in the PCEs of the BHJSCs with TA or TA+SVA treated active layers could be due to better nanoscale morphology of the active layer induced by annealing treatment. To ascertain this, X-ray diffraction (XRD) and atomic force microscopy (AFM) analyses were performed. XRD patterns of the active layer blend thin films processed under different conditions are provided in Fig. 8. As shown in Fig. 8, ICT3:PC₇₁BM blend thin film as cast from chloroform solvent displayed a strong (100) reflection peak at approximately around $2\theta = 5.08^\circ$, corresponding to d_{100} spacing of 17.38 Å. The peak at small angle suggests that d_{100} spacing is between the side chain rather than π - π stacking and indicates that the molecular packing is dominated by the alkyl side chains of ICT3.²¹ TA or TA+SVA treatment of the active layer appreciably altered the XRD pattern of the blend thin films and we observed significant enhancement in the reflection intensity of the diffraction peak, indicating that TA or TA+SVA treatment improves the degree of crystallinity of the active layer. Enhanced crystallinity is beneficial for the carrier transport and collection and reduced charge recombination, resulting in an improvement in J_{sc} of the resulted device. AFM images of the ICT3:PC₇₁BM blend thin film are shown in Fig. 9. As cast ICT3:PC₇₁BM blend thin film showed a uniform surface morphology with surface roughness root mean square (RMS) value of 0.74 nm, indicating that observed nanoscale morphology is not sufficient for efficient exciton dissociation due to the reduced D-A interface area. Also these smaller domains can hinder the charge transport due to insufficient interpenetrating pathways, increase in the charge carrier recombination and leads to poor J_{sc} and FF values. However, with TA+SVA treatment, the RMS value of ICT3:PC₇₁BM blend thin film is increased to 1.26 nm, indicating more ordered packing in the active layer.^{67,77} The increment in the RMS value may lead to better phase separation and proper domain size of donor and acceptor molecules in the active layer, which is

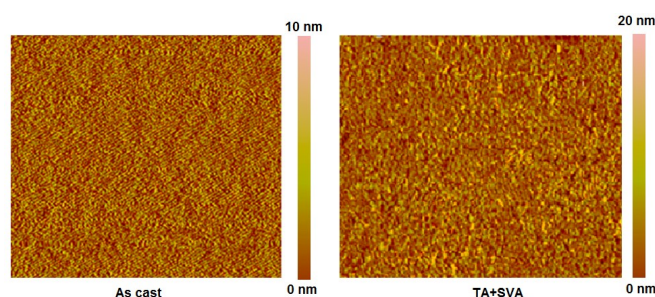


Fig. 9 AFM images of as cast and TA+SVA treated ICT3:PC₇₁BM active layers. Image size is 3 μ m x 3 μ m

beneficial for exciton dissociation and charge transport, and it could be the reason for the improvement in overall PCE of the BHJSCs.⁷⁸ Hence all these experiments collectively demonstrate that TA+SVA treatment of active layer induces crystallinity and better nanoscale morphology to the active layer and improves the device exciton generation and dissociation efficiency, charge transport and collection efficiency and reduces carrier recombination.

Conclusion

In summary, we have synthesized a novel low band gap organic small molecular donor material, ICT3 with A-D-D-D-A architecture using DTP and butylrhodanine as donor and acceptor moieties. Thermal, photophysical, electrochemical and photovoltaic properties of ICT3 are explored. ICT3 is stable over a broad range of temperatures, suitable for solution processing during device fabrication and it has suitable HOMO and LUMO energy levels compared to PC₇₁BM acceptor. BHJSCs are fabricated using ICT3 as donor and PC₇₁BM as acceptor materials and devices with the active layer as cast from chloroform solvent displayed PCE of 3.04 %. Annealing treatment of the active layer significantly improved the PCE of the BHJSCs. BHJSCs with TA treated active layer exhibited PCE of 4.94 % and it is 6.53 % for the BHJSCs with TA+SVA treated active layer. XRD and AFM analyses on the active layer revealed that annealing treatment improves the crystallinity and nanoscale morphology of the active layer and enrich the device exciton generation and dissociation efficiency, charge transport and collection efficiency and reduces carrier recombination. Observed higher PCE (6.53 %) associated with the BHJSCs having ICT3 with DTP donor moiety broadens the scope to develop new, efficient DTP based small molecular donor materials for BHJSCs.

Acknowledgements

N. R. Chereddy thanks the DST, India, for INSPIRE faculty Fellowship. B. M. Reddy and B. Shanigaram thank the UGC and CSIR, India, for research fellowship. Financial support from CSIR project NWP0054 is greatly acknowledged.

Notes and references

- 1 A. J. Heeger, *Chem. Soc. Rev.*, 2010, **39**, 2354.
- 2 Y. Li, *Acc. Chem. Res.*, 2012, **45**, 723.
- 3 F. C. Krebs, *Sol. Energy Mater. Sol. Cells*, 2009, **93**, 394.
- 4 Y. Liu, X. Wan, F. Wang, J. Zhou, G. Long, J. Tian, J. You, Y. Yang and Y. Chen, *Adv. Energy Mater.*, 2011, **1**, 771.
- 5 J. Zhou, Y. Zuo, X. Wan, G. Long, Q. Zhang, W. Ni, Y. Liu, Z. Li, G. He, C. Li, B. Kan, M. Li and Y. Chen, *J. Am. Chem. Soc.*, 2013, **135**, 8484.
- 6 L. Dou, J. You, Z. Hong, Z. Xu, G. Li, R. A. Street and Y. Yang, *Adv. Mater.*, 2013, **25**, 6642.
- 7 Q. Zhang, B. Kan, F. Liu, G. Long, X. Wan, X. Chen, Y. Zuo, W. Ni, H. Zhang, M. Li, Z. Hu, F. Huang, Y. Cao, Z. Liang, M. Zhang, T. P. Russell and Y. Chen, *Nat. Photonics*, 2014, **9**, 35.
- 8 Y. Liu, C.-C. Chen, Z. Hong, J. Gao, Y. Yang, H. Zhou, L. Dou, G. Li and Y. Yang, *Sci. Rep.*, 2013, **3**, 3356.

- 9 J. Hou, H.-Y. Chen, S. Zhang, G. Li and Y. Yang, *J. Am. Chem. Soc.*, 2008, **130**, 16144. View Article Online
DOI: 10.1039/C6CP06304G
- 10 M. Morana, H. Azimi, G. Dennler, H.-J. Egelhaaf, M. Scharber, M. Forberich, J. Hauch, R. Gaudiana, D. Waller, Z. Zhu, K. Hingerl, S. S. van Bavel, J. Loos and C. J. Brabec, *Adv. Funct. Mater.*, 2010, **20**, 1180.
- 11 M. C. Scharber, M. Koppe, J. Gao, F. Cordella, M. A. Loi, P. Denk, M. Morana, H.-J. Egelhaaf, K. Forberich, G. Dennler, R. Gaudiana, D. Waller, Z. Zhu, X. Shi and C. J. Brabec, *Adv. Mater.*, 2010, **22**, 367.
- 12 H.-Y. Chen, J. Hou, A. E. Hayden, H. Yang, K. N. Houk and Y. Yang, *Adv. Mater.*, 2010, **22**, 371.
- 13 R. C. Coffin, J. Peet, J. Rogers and G. C. Bazan, *Nat. Chem.*, 2009, **1**, 657.
- 14 B. Walker, C. Kim and T. Q. Nguyen, *Chem. Mater.*, 2011, **23**, 470.
- 15 B. O'Regan and M. Gratzel, *Nature*, 1991, **353**, 737.
- 16 D. Bharath, S. Chithiravel, M. Sasikumar, N. R. Chereddy, B. Shanigaram, K. Bhanuprakash, K. Krishnamoorthy and V. J. Rao, *RSC Adv.*, 2015, **5**, 94859.
- 17 P. Gautam, R. Misra and G. D. Sharma, *Phys. Chem. Chem. Phys.*, 2016, **18**, 7235.
- 18 Y. Patil, R. Misra, A. Sharma and G. D. Sharma, *Phys. Chem. Chem. Phys.*, 2016, **18**, 16950.
- 19 Y. Patil, R. Misra, F. C. Chen and G. D. Sharma, *Phys. Chem. Chem. Phys.*, 2016, **18**, 22999.
- 20 P. Gautam, R. Misra, S. Biswas and G. D. Sharma, *Phys. Chem. Chem. Phys.*, 2016, **18**, 13918.
- 21 P. Gautam, R. Misra, S. A. Siddiqui and G. D. Sharma, *ACS Appl. Mater. Interfaces*, 2015, **7**, 10283.
- 22 H. Chen, J. Hou, S. Zhang, Y. Liang, G. Yang, Y. Yang, L. Yu, Y. Wu and G. Li, *Nat. Photonics*, 2009, **3**, 649.
- 23 K. Vandewal, K. Tvingstedt, A. Gadisa, O. Inganäs and J. V. Manca, *Nat. Mater.*, 2009, **8**, 904.
- 24 H.-I. Lu, C.-W. Lu, Y.-C. Lee, H.-W. Lin, L.-Y. Lin, F. Lin, J.-H. Chang, C.-I. Wu and K.-T. Wong, *Chem. Mater.*, 2014, **26**, 4361.
- 25 J. Yuan, X. Huang, F. Zhang, J. Lu, Z. Zhai, C. Di, Z. Jiang and W. Ma, *J. Mater. Chem.*, 2012, **22**, 22734.
- 26 H. Zhou, L. Yang, A. C. Stuart, S. C. Price, S. Liu and W. You, *Angew. Chem., Int. Ed.*, 2011, **50**, 2995.
- 27 Y. Liu, X. Wan, F. Wang, J. Zhou, G. Long, J. Tian and Y. Chen, *Adv. Mater.*, 2011, **23**, 5387.
- 28 S. Shen, P. Jiang, C. He, J. Zhang, P. Shen, Y. Zhang, Y. Yi, Z. Zhang, Z. Li and Y. Li, *Chem. Mater.*, 2013, **25**, 2274.
- 29 B. M. Reddy, M. V. N. Raju, N. R. Chereddy, B. Shanigaram, K. Bhanuprakash, S. Biswas, G. D. Sharma and V. J. Rao, *Org. Electron.*, 2016, **37**, 312.
- 30 S. C. Rasmussen and S. J. Evenson, *Prog. Polym. Sci.*, 2013, **38**, 1773.
- 31 A. Yassin, T. Rousseau, P. Leriche, A. Cravino and J. Roncali, *Sol. Energy Mater. Sol. Cells*, 2011, **95**, 462.
- 32 R. Grisorio, G. Allegretta, G. P. Suranna, P. Mastroilli, A. Loiudice, A. Rizzo, M. Mazzeo and G. Gigli, *J. Mater. Chem.*, 2012, **22**, 19752.
- 33 A. Yassin, G. Savitha, P. Leriche, P. Frere and J. Roncali, *New J. Chem.*, 2012, **36**, 2412.
- 34 A. Yassin, P. Leriche, M. Allain and J. Roncali, *New J. Chem.*, 2013, **37**, 502.
- 35 B. H. Wunsch, Ma. Rumi, N. R. Tummala, C. Risko, D.-Y. Kang, K. X. Steirer, J. Gantz, M. Said, N. R. Armstrong, J.-L. Brédas, D. Bucknall and S. R. Marder, *J. Mater. Chem. C*, 2013, **1**, 5250.
- 36 M. Weidelener, C. D. Wessendorf, J. Hanisch, E. Ahlswede, G. Gotz, M. Linden, G. Schulz, E. Mena-Osteritz, A. Mishra and P. Bauerle, *Chem. Commun.*, 2013, **49**, 10865.
- 37 Q.-C. Yu, W.-F. Fu, J.-H. Wan, X.-F. Wu, M.-M. Shi and H.-Z. Chen, *ACS Appl. Mater. Interfaces*, 2014, **6**, 5798.

- 38 L. G. Mercier, A. Mishra, Y. Ishigaki, F. Henne, G. Schulz and P. Bauerle, *Org. Lett.*, 2014, **16**, 2642.
- 39 A. Mishra, D. Popovic, A. Vogt, H. Kast, T. Leitner, K. Walzer, M. Pfeiffe, E. Mena-Osteritz and P. Bäuerle, *Adv. Mater.*, 2014, **26**, 7217.
- 40 H. Kast, A. Mishra, G. L. Schulz, M. Urdanpilleta, E. Mena-Osteritz and P. Bäuerle, *Adv. Funct. Mater.*, 2015, **25**, 3414.
- 41 G. L. Schulz, M. Lobert, I. Ata, M. Urdanpilleta, M. Linden, A. Mishra and P. Bauerle, *J. Mater. Chem. A*, 2015, **3**, 13738.
- 42 C. D. Wessendorf, A. Perez-Rodriguez, J. Hanisch, A. P. Arndt, I. Ata, G. L. Schulz, A. Quintilla, P. Bauerle, U. Lemmer, P. Wochner, E. Ahlswede and E. Barren, *J. Mater. Chem. A*, 2016, **4**, 2571.
- 43 C. Wetzal, A. Mishra, E. Mena-Osteritz, K. Walzer, M. Pfeiffer and P. Bäuerle, *J. Mater. Chem. C*, 2016, **4**, 3715.
- 44 K. Wang, M. Azouz, M. Babics, F. Cruciani, T. Marszalek, Q. Saleem, W. Pisula and P. M. Beaujuge, *Chem. Mater.*, 2016, **28**, 5415.
- 45 X. Che, C.-L. Chung, X. Liu, S.-H. Chou, Y.-H. Liu, K.-T. Wong and S. R. Forrest, *Adv. Mater.*, 2016, DOI: 10.1002/adma.201601957.
- 46 S. P. Mishra, A. K. Palai, R. Srivastava, M. N. Kamalasanan and M. Patri, *J. Polym. Sci., Part A: Polym. Chem.*, 2009, **47**, 6514.
- 47 G. Lu, H. Usta, C. Risko, L. Wang, A. Facchetti, M. A. Ratner and T. J. Marks, *J. Am. Chem. Soc.*, 2008, **130**, 7670.
- 48 K. Ogawa and S. C. Rasmussen, *Macromolecules*, 2006, **39**, 1771.
- 49 L. Zhang, M. Pu, W. Zhou, X. Hu, Y. Zhang, Y. Xie, B. Liu and Y. Chen, *J. Phys. Chem. C*, 2015, **119**, 23310.
- 50 A. Yassin, P. Leriche and J. Roncali, *Macromol. Rapid Commun.*, 2010, **31**, 1467.
- 51 K.-H. Kim, H. Yu, H. Kang, D. J. Kang, C.-H. Cho, H.-H. Cho, J. H. Oh and B. J. Kim, *J. Mater. Chem. A*, 2013, **1**, 14538.
- 52 N. Herath, S. Das, J. K. Keum, J. Zhu, R. Kumar, I. N. Ivanov, B. G. Sumpter, J. F. Browning, K. Xiao, G. Gu, P. Joshi, S. Smith and V. Lauter, *Sci. Rep.*, 2015, **5**, 13407.
- 53 J. Liu, Y. Sun, P. Moonsin, M. Kuik, C. M. Proctor, J. Lin, B. B. Hsu, V. Promarak, A. J. Heeger and T.-Q. Nguyen, *Adv. Mater.*, 2013, **25**, 5898.
- 54 J. M. Szarko, B. S. Rolczynski, S. J. Lou, T. Xu, J. Strzalka, T. J. Marks, L. Yu and L. X. Chen, *Adv. Funct. Mater.*, 2014, **24**, 10.
- 55 C.W. Tang, *Appl. Phys. Lett.*, 1986, **48**, 183.
- 56 A. D. Becke, *Phys. Rev. A*, 1988, **38**, 3098.
- 57 A. D. Becke, *J. Chem. Phys.*, 1993, **98**, 5648.
- 58 C. Lee, W. Yang and R. G. Parr, *Phys. Rev. B*, 1988, **37**, 785.
- 59 P. C. Hariharan and P. A. Pople, *Theor. Chim. Acta*, 1973, **28**, 213.
- 60 M. M. Francl, W. J. Pietro, W. J. Hehre, J. S. Binkley, M. S. Gordon, D. J. DeFrees and J. A. Pople, *J. Chem. Phys.*, 1982, **77**, 3654.
- 61 V. A. Rassolov, J. A. Pople, M. A. Ratner and T. L. Windus, *J. Chem. Phys.*, 1998, **109**, 1223.
- 62 J. P. Perdew, K. Burke and M. Ernzerhof, *Phys. Rev. Lett.*, 1996, **77**, 3865.
- 63 Y. Zhao and D. G. Truhlar, *Theor. Chem. Acc.*, 2008, **120**, 215.
- 64 M. Cossi, V. Barone, R. Cammi and J. Tomasi, *Chem. Phys. Lett.*, 1996, **255**, 327.
- 65 M. J. Frisch, G. W. Trucks, H. B. Schlegel, G. E. Scuseria, M. A. Robb, J. R. Cheeseman, G. Scalmani, V. Barone, B. Mennucci and G. A. Petersson, et al., Gaussian 09, Revision B.01, Gaussian, Inc., Wallingford, CT, 2010.
- 66 N. M. O'Boyle, A. L. Tenderholt and K. M. Langner, *J. Comp. Chem.*, 2008, **29**, 839.
- 67 B. Kan, Q. Zhang, M. Li, X. Wan, W. Ni, G. Long, Y. Wang, X. Yang, H. Feng and Y. Chen, *J. Am. Chem. Soc.*, 2014, **136**, 15529.
- 68 A. K. K. Kyaw, D. H. Wang, C. Luo, Y. Cao, T. O. Nguyen, G. C. Bazan and A. J. Heeger, *Adv. Energy Mater.*, 2014, **4**, 1301469.
- 69 J.-L. Wang, F. Xiao, J. Yan, Z. Wu, K.-K. Liu, Z.-F. Chang, R.-B. Zhang, H. Chen, H.-B. Wu and Y. Cao, *Adv. Funct. Mater.*, 2016, **26**, 1803.
- 70 D. Wang, F. Liu, N. Yagihashi, M. Nakaya, S. Ferdous, X. Liang, A. Muramatsu, K. Nakajima and T. P. Russell, *Nano Lett.*, 2014, **14**, 5727.
- 71 J. Sim, K. Do, K. Song, A. Sharma, S. Biswas, G. D. Sharma and J. Ko, *Org. Electron.*, 2016, **30**, 122.
- 72 M. Kiy, P. Losio, I. Biaggio, M. Koehler, A. Tapponnier and P. Günter, *Appl. Phys. Lett.*, 2002, **80**, 1198.
- 73 P. W. M. Blom, V. D. Mihailetschi, L. J. A. Koster and D. E. Markov, *Adv. Mater.*, 2007, **19**, 1551.
- 74 V. D. Mihailetschi, H. X. Xie, B. de Boer, L. J. A. Koster and P. W. M. Blom, *Adv. Funct. Mater.*, 2006, **16**, 699.
- 75 V. Shrotriya, Y. Yao, G. Li and Y. Yang, *Appl. Phys. Lett.*, 2006, **89**, 063505.
- 76 Z. He, C. Zhong, X. Huang, W.-Y. Wong, H. Wu, L. Chen, S. Su and Y. Cao, *Adv. Mater.*, 2011, **23**, 4636.
- 77 B. Qiu, J. Yuan, Y. Zou, D. He, H. Peng, Y. Li and Z. Zhang, *Org. Electron.*, 2016, **35**, 87.
- 78 Z. Guo, D. Lee, R. D. Schaller, X. Zuo, B. Lee, T. Luo, H. Gao and L. Huang, *J. Am. Chem. Soc.*, 2014, **136**, 10024.